

Operational Wave Prediction System at Environment Canada: Going Global to Improve Regional Forecast Skill

NATACHA B. BERNIER

Recherche en Prévision Numérique Environnementale, Environment Canada, Dorval, Quebec, Canada

JOSE-HENRIQUE G. M. ALVES, HENDRIK TOLMAN, AND ARUN CHAWLA

NOAA Center for Weather and Climate Prediction, College Park, Maryland

SYD PEEL, BENOIT POULIOT, JEAN-MARC BÉLANGER, AND PIERRE PELLERIN

Recherche en Prévision Numérique Environnementale, Environment Canada, Dorval, Quebec, Canada

MARIO LÉPINE

Services Informatiques de Recherche, Environment Canada, Dorval, Quebec, Canada

MICHEL ROCH

Recherche en Prévision Numérique Atmosphérique, Environment Canada, Dorval, Quebec, Canada

(Manuscript received 3 July 2015, in final form 18 September 2015)


ABSTRACT

A global deterministic wave prediction system (GDWPS) is used to improve regional forecasts of waves off the Canadian coastline and help support the practice of safe marine activities in Canadian waters. The wave model has a grid spacing of $1/4^\circ$ with spectral resolution of 36 frequency bins and 36 directional bins. The wave model is driven with hourly 10-m winds generated by the operational global atmospheric prediction system. Ice conditions are updated every three hours using the ice concentration forecasts generated by the Global Ice–Ocean Prediction System. Wave forecasts are evaluated over two periods from 15 August to 31 October 2014 and from 15 December 2014 to 28 February 2015, as well as over select cases during the fall of 2012. The global system is shown to improve wave forecast skill over regions where forecasts were previously produced using limited-area models only. The usefulness of a global expansion is demonstrated for large swell events affecting the northeast Pacific. The first validation of a Canadian operational wave forecast system in the Arctic is presented. Improvements in the representation of forecast wave fields associated with tropical cyclones are also demonstrated. Finally, the GDWPS is shown to result in gains of at least 12 h of lead time.

1. Introduction

Canadian Pacific, Arctic, and Atlantic waters are the site of extensive commercial and recreational shipping, fishing, and boating activities. Navigation accidents are

numerous each year. Western Canadian waters are plagued with the most accidents followed closely by the Maritimes and Newfoundland ([Transportation Safety Board of Canada 2010](#)). More than half of the vessels registered in Canadian waters are fishing vessels. They account for nearly half of the few hundred accidents reported annually and result in the loss of more than 10 lives per year ([Transportation Safety Board of Canada 2010](#)). Vessel types and the accidents they are involved in are varied. For example, in 1904 the Clallam ferry sank in a storm off of British Columbia, taking 56 lives ([The Daily Colonist 1904](#)). In 1982, the semisubmersible Ocean Ranger and its 84 crew members were taken by a rapidly

 Denotes Open Access content.

Corresponding author address: Natacha B. Bernier, Recherche en Prévision Numérique Environnementale (RPN-E), Environment Canada, 2121 Route Trans-Canadienne, Dorval QC H9P 1J3, Canada.
E-mail: natacha.bernier@ec.gc.ca

DOI: 10.1175/WAF-D-15-0087.1

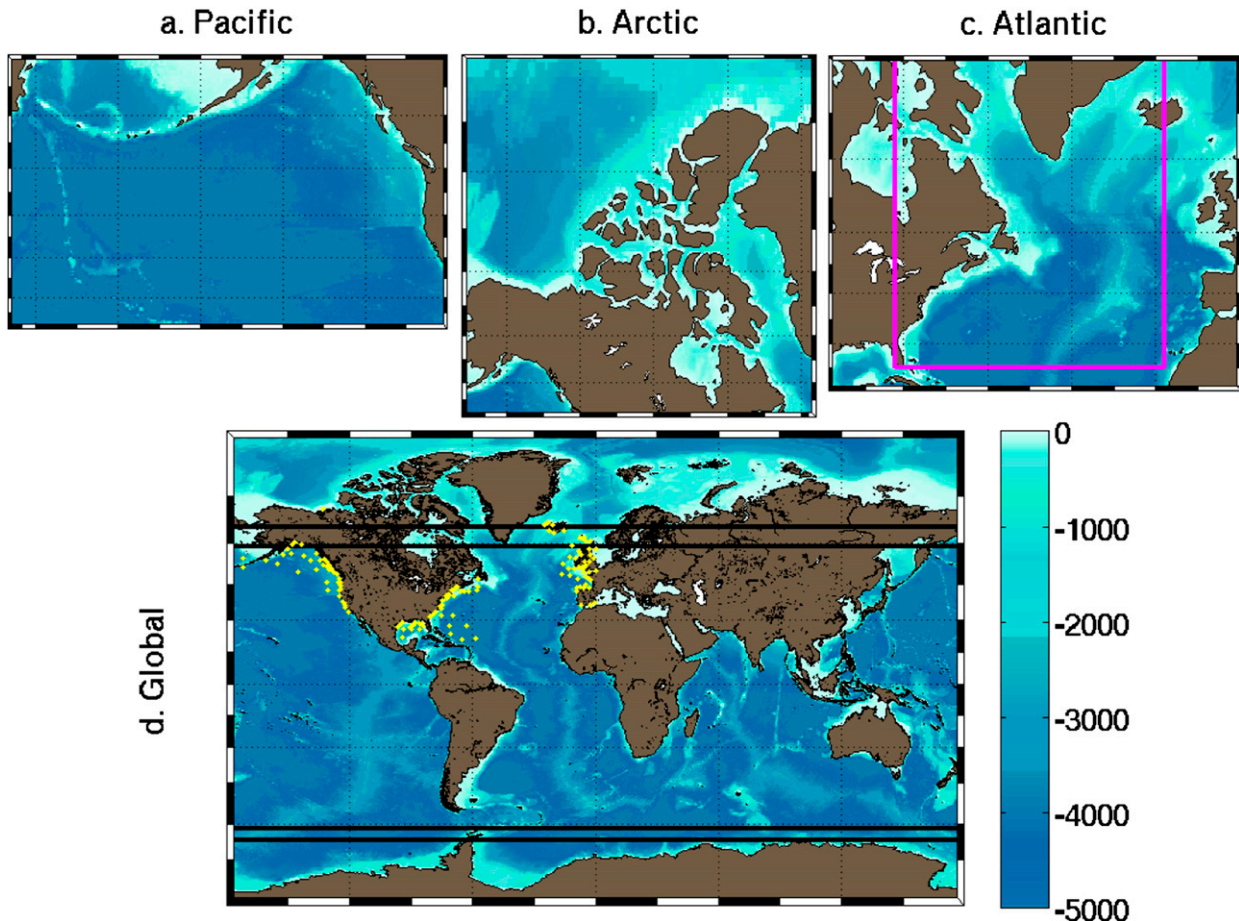


FIG. 1. Domain of the regional and global deterministic wave prediction systems. Colors indicate depth in meters. The domain of the regional (a) Pacific, (b) Arctic, and (c) short-range Atlantic and long-range Atlantic (magenta box) wave forecast systems. (d) The global deterministic system. The black lines represent overlapping regions between polar and equatorial grids (section 2b). The yellow dots mark the location of buoys described in section 3a that fall within the common region covered by the regional systems and the GDWPS.

approaching storm bringing 30-m waves (CBCnews 2012). In the 1991 “perfect storm,” the Andrea Gail sank in the rough seas off Sable Island taking its six crew members (Out of Gloucester 1991). More recently, on 17 February 2013, five fishermen perished off the coast of Nova Scotia when their vessel capsized after experiencing hazardous sea states (CBCnews 2013). With ongoing fishing, intensified oil and gas exploration, growing tourism, and increased maritime cargo transport, the development and implementation of improved marine forecasts remains a priority.

Worldwide, wave forecasting continues to receive considerable attention from both the research and operational communities (e.g., Tolman et al. 2013). Several countries have already developed and implemented global wave forecast systems—for example, the European Center for Medium-Range Weather Forecasts [Bidlot (2012) and references therein], the Met Office (Li and Saulter 2014), the U.S. Navy (Rogers et al.

2014), and the National Centers for Environmental Prediction (Chawla et al. 2013), and additional centers are participating in the intercomparison of operational wave forecasting systems such as the Japanese Meteorological Agency, the Korean Meteorological Administration, and the Australian Bureau of Meteorology (Bidlot et al. 2007). In Canada, operational development has historically been limited to regional forecast systems (Figs. 1a,b,c, and the Great Lakes; not shown), until the recent implementation of the global wave forecast system (Fig. 1d) described in this article.

Environment Canada (EC) began producing regional numerical wave guidance in 1991 using the first-generation Canadian Spectral Ocean Wave Model (CSOWM; Khandekar and Lalbeharry 1996). In 1996, the Wave Model (WAM; The WAMDI Group 1988) replaced the CSOWM in operations. Since then, upgrades to regional wave forecast systems included an upgrade to WAM cycle 4.5.1, the addition of regional

TABLE 1. Details of the regional and global wave prediction systems. The RDPS and GDPS are the atmospheric systems described in section 4a. GIOPS is the ice–ocean model described in section 4b.

Domain	Lat and lon	Grid spacing	Forecast range		Ice	Runs per day
			10-m winds			
Regional wave prediction systems						
Pacific (long range)	200°–120°W, 25°–60°N	0.5° × 0.5°	120 h	GDPS 3 hourly	GDPS ice analysis	0000 and 1200 UTC
Arctic (long range)	165°–45°W, 49°–85°N	0.4° × 0.8°	120 h	GDPS 3 hourly	GDPS ice analysis	0000 and 1200 UTC
Arctic (short range)	165°–45°W, 49°–85°N	0.4° × 0.8°	48 h	RDPS hourly	RDPS ice analysis	0000, 0600, 1200, and 1800 UTC
Atlantic (long range)	82°–15°W, 25°–70°N	0.5° × 0.5°	120 h	GDPS 3 hourly	GDPS ice analysis	0000 and 1200 UTC
Atlantic (short range)	97.925°W–0.25°E, 20.075°S–70.175°N	0.15° × 0.15°	48 h	RDPS hourly	RDPS ice analysis	0000, 0600, 1200, and 1800 UTC
Global deterministic wave prediction systems (GDWPS)						
Global (pseudoanalysis)	0°–360°, 80°S–86°N	0.25° × 0.25°	6 h	Late GDPS analysis hourly	GIOPS 3 hourly	0000, 0600, 1200, and 1800 UTC
Global (long range)	0°–360°, 80°S–86°N	0.25° × 0.25°	120 h	GDPS hourly	GIOPS 3 hourly	0000 and 1200 UTC

domains covering the Great Lakes and part of the Arctic Ocean, increased horizontal resolution for two select regions (i.e., the northwest Atlantic and Gulf of St. Lawrence), and increases of forecast lead time to 120 h [see CMC (2012) for details] although there remains no guidance, other than raw forecast fields, issued beyond 48 h.

The present study has four primary objectives: (i) Describe the development of the Canadian Global Deterministic Wave Prediction System (GDWPS) and the improvements it brings over the regional domains historically used. These improvements include increased horizontal and spectral resolutions, the inclusion of time-evolving ice fields, upgrades to the physics package, and a better representation of the atmospheric forcing. (ii) Evaluate, for the first time, the Canadian operational wave forecasts within the Arctic Ocean. Both in situ and satellite observations are used to discuss forecast skill. (iii) Fix the long-standing issue of poorly forecast swell seas on the northeast Pacific coast. We will demonstrate that the increased spatial coverage of the global domain allows coverage of areas of swell formation that can then propagate to the eastern Pacific coastline. And (iv) improve forecast wave fields associated with tropical cyclones.

The regional wave models previously used for wave guidance and the global wave models used for wave forecasts are described in section 2. The wave observations are summarized in section 3. The wave forecast cycle, including the generation of the atmospheric forcing fields and of the ice conditions, is described in section 4. The validation of the regional and global wave forecasts against moored buoys and satellite data is presented in

section 5, and the results of the study are summarized and discussed in the final section.

2. Wave prediction models

Figure 1 shows the regional forecast domains (Figs. 1a–c) that are being replaced with the global domain (Fig. 1d). Both are briefly described in this section.

a. The limited-area domain wave forecast models

The regional forecast system comprises five domains (excluding the Great Lakes). Two lead times exist for these regional systems: (i) short range (48 h) and (ii) long range (120 h). Two short-range regional forecast systems (Arctic and Atlantic; see Table 1 for details) are driven with hourly 10-m winds provided by the Regional Deterministic Prediction System (RDPS; see section 4a for details). Ice conditions result from the operational ice analysis and are held static throughout the wave forecast's integration. They are produced with WAM cycle 4.5.1 and are run four times daily at 0000, 0600, 1200, and 1800 UTC.

Long-range regional forecast systems (Pacific, Arctic, and Atlantic; see Table 1 for details) are driven using 3-hourly 10-m winds from the Global Deterministic Prediction System (GDPS; see section 4a for details). Ice conditions for the long-range wave forecasts are held static and taken from the operational ice analysis. The long-range wave forecasts are integrated twice daily at 0000 and 1200 UTC using WAM cycle 4.5.

Initial conditions of short-range and long-range wave forecasts are the results of the most recent forecast available for the time at which the new run begins.

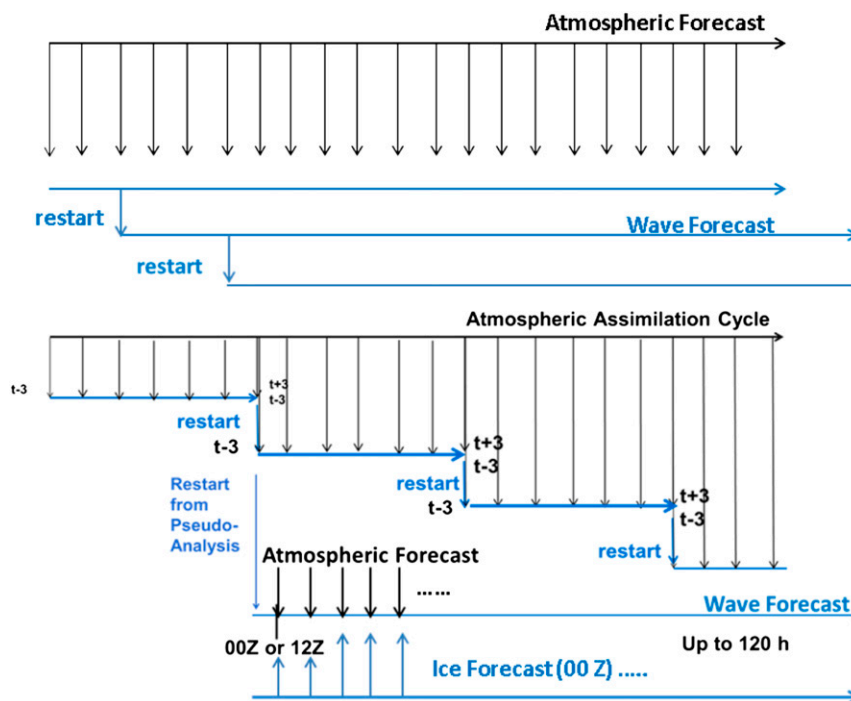


FIG. 2. Schematic of the (top) regional and (bottom) global wave prediction systems. Atmospheric forecast refers to either the RDPS or GDPS; similarly, wave forecast refers to either the regional wave forecast systems or the GDWPS. For the regional system, restarts are produced every 6 or 12 h (see Table 1 and section 2a for details). For the GDWPS, the pseudoanalysis is driven with the hourly atmospheric assimilation cycle fields from which restarts are taken every 6 h. The GDWPS forecasts are then driven by the global atmospheric and global ice–ocean prediction systems (see Table 1 and section 2b for details).

Hence, in the case of the shorter-range forecasts (i.e., 48 h), the forecast from hour 6 of the previous run is used to initialize the current forecast run as shown in Fig. 2a. Similarly, for the long-range forecasts (i.e., 120 h), the forecast from hour 12 of the previous run is used to initialize the current run (Fig. 2a).

The regional short-range and long-range wave forecast systems operate with a spectral resolution of 25 frequency bins (ranging from 0.0417 Hz to 0.411 Hz in increments of 1.10) and 24 directional bins of 15° each (Table 1). The long-range Pacific domain extends from 200° to 120°W and 25° to 60°N with grid spacing of 0.5° × 0.5°. Both the short-range and long-range Arctic domains (Fig. 1b) extend from 165° to 45°W and 49° to 85°N with grid spacing of 0.4° × 0.8°. In the Atlantic (Fig. 1c), there are two domains. The larger domain is the short-range domain. It extends from 97.925°W to 0.25°E and 20.075° to 70.175°N with grid spacing of 0.15° × 0.15°. The smaller domain (delimited with the magenta box; Fig. 1c) is the long-range domain. It extends from 82° to 18°W and 25° to 70°N with the coarser grid spacing of 0.5° × 0.5°. Thus,

the smaller domain is used to produce the longer-range guidance.

b. The global wave forecast model

The GDWPS was developed and tested using WAVEWATCH III v4.18 (hereafter WW3; Tolman et al. 2014). Wave fields are computed by solving the linear balance equation for the spectral wave action density. Parameterizations for wind input and dissipation due to whitecapping, opposing swells, long–short wind–wave interactions, and wave–turbulence interaction are computed using the source terms of Ardhuin et al. (2010). The default source term settings are used except for β_{\max} , which is set to 1.5 following a slight retuning of the wind source function for applications using EC’s global deterministic wind fields. Nonlinear wave–wave interactions are computed using the discrete interaction approximation (DIA; Hasselmann et al. 1985). The Joint North Sea Wave Project (JONSWAP) parameterization for bottom friction (Hasselmann et al. 1973), depth-induced wave breaking (Battjes and Janssen 1978), and default

propagation and averaging for alleviation of the garden sprinkler effect (Tolman 2003) are also used.

Wave–ice interactions in the wave model are parameterized with an ice concentration above 25% resulting in gradual decay. Once the ice concentration exceeds 75%, the ice cover is treated like a land surface such that wave energy is assumed to be zero and boundaries at ice edges are treated like boundaries along shorelines (Tolman 2003).

The GDWPS covers from 80°S to 86°N on a regular spherical latitude–longitude grid with a spacing of $0.25^\circ \times 0.25^\circ$ (Fig. 1d). The maximum time step is limited by the CFL criterion and so operating in polar regions is expensive. The overlapping grid method of Tolman (2008), which allows two-way nesting, is used to reduce the size of areas for which short time steps are applied. For the GDWPS three overlapping grids are used: (i) the northern grid extends from 59° to 86°N, (ii) the center grid extends from 65°S to 65°N, and (iii) the southern grid extends from 80° to 61.5°S (Fig. 1d, black lines). All three grids are run simultaneously with resources assigned such that they require approximately the same time to compute (thus reducing CPU idle time). Propagation of the information across the overlapping region is performed at the longest common time step (i.e., at the time step of the center grid). Using the selected three domain configuration, savings amount to roughly 15% of the computing resources needed to run the system. The spectral resolution is made of 36 bins of direction (of 10° each) and 36 bins of frequency (ranging from 0.035 Hz to 0.984 Hz in increments of 1.10). A parametric tail is fitted for higher frequencies. Gridgen, a MATLAB routine developed by Chawla and Tolman (2007), was used to prepare the bathymetry and obstruction points [as described by Chawla and Tolman (2008)]. The ETOPO1 bathymetry (Amante and Eakins 2009) and the Global Self-consistent, Hierarchical, High-resolution, Shoreline database (GSHHS; Wessel and Smith 1996) were used as input for gridgen.

The forecast cycle of the GDWPS has also been updated. In lieu of the setup used for the regional systems, where initial conditions result from the previous forecast run (see section 2a and Fig. 2a), a pseudoanalysis cycle has been added. For the moment, there is no wave data assimilation performed. The wave analysis is simply driven using hourly analyzed winds and analyzed ice fields, hence the term pseudoanalysis. The pseudoanalysis is run four times daily centered on 0000, 0600, 1200, and 1800 UTC driven with hourly conditions from a late atmospheric forecast analysis performed at a later cutoff time to allow for the arrival of more observations (section 4a). Each new pseudoanalysis is

simply a smooth continuation of the previous run. The initial conditions of the forecast runs are the result of the latest available pseudoanalysis. The GDWPS 120-h forecast cycle is run twice daily at 0000 and 1200 UTC. It is driven with hourly 10-m winds from the GDPS (section 4a) and 3-hourly ice forecasts from the Global Ice–Ocean Prediction System (GIOPS; section 4b). We note that the forcing fields are carefully mapped to the wave grid using the atmospheric model land–sea interface to first spread wind speeds from ocean points onto the land points adjacent to the land–sea interface. This step is motivated by the tendency to find weaker winds at the coastline due to the increased land surface friction. Failing to correct for this effect can result in low biased wind speeds along the coastline. The interpolation of the wind speeds is then performed to produce the forcing fields. The usefulness of this correction depends on differences in the resolution of the forcing and forced models as well as the position of their respective land–sea interface. In polar regions, where the grid spacing of the atmospheric and wave model differ significantly (owing primarily to increasing differences with latitude in their grids, the atmospheric model grid being uniform globally), this effect can be felt over up to a few grid points.

3. Wave observations

Two sources of wave observation—moored buoy and satellite altimeter data—were used to validate and compare the wave forecast systems. They are briefly described below.

a. Moored buoys

The moored buoy datasets discussed in this study are those kindly collected and distributed monthly to participating centers of the international buoy intercomparison (Bidlot et al. 2002, 2007). In general, a subset of the buoys is used for the international intercomparison of significant wave height H_s and peak period T_p . Here, all buoys located at least one model grid point away from the wave model land–sea interface and within one of the regions common to the regional and GDWPS systems were visually examined (yellow dots on Fig. 1d). Many records were incomplete over the period of interest; those with only several observations were rejected. A number of records were also found to report unrealistic spikes. Clearly erroneous observations were removed prior to further processing. All remaining records were used for validation. It is noted that buoys reporting mean wave period (mostly European buoys) were used only for the validation of significant wave height. Two buoy records from stations 48213

(Burger; MOB2) and 48214 (Klondike; MOB1) in the Arctic Ocean were added to the dataset described above. The records were obtained from the National Data Buoy Center (www.ndbc.noaa.gov). They are the only in situ observations available in the record low Arctic ice season of 2012. In addition, observed spectra from buoys 46213 (Cape Mendocino) and 46246 (station Papa) were acquired from the Coastal Data Information Program (cdip.ucsd.edu).

b. Satellite altimeter observation

Significant wave heights from satellite observation were also used to validate the wave models. The GlobWave (globwave.ifremer.fr) merged dataset (Queffelec 2004) was used. The merged set contains data from several altimeters. For the periods of interest, *Jason-2*, *Cryosphere Satellite-2* (*CryoSAT-2*), and *Satellite with Argos and AltiKa* (*SARAL*) were available. *SARAL* and *CryoSAT-2* were particularly useful in providing much-needed data in the Arctic Ocean for which there is little in situ wave observation.

4. The forcing fields

The regional and global atmospheric forecast systems that provide the forcing fields for the wave forecast systems are discussed in section 4a. The global ocean–ice system from which time varying ice fields are taken is described in section 4b.

a. Regional and global atmospheric forecasts

The forecast component [global environmental multi-scale (GEM)] of both the RDPS and GDPS was developed at Environment Canada by Côté et al. (1998a,b). Over the years, GEM has undergone many upgrades. The RDPS is now integrated on a grid spacing of approximately 10 km. In the GDPS, GEM now operates at a grid spacing of approximately 25 km, on a vertically staggered Charney–Phillips grid (Charney and Phillips 1953), with a log-hydrostatic pressure coordinate (Girard et al. 2014).

The preparation of analyses has recently undergone a major upgrade. It is now based on ensemble–variational data assimilation at the regional and global scales [Caron et al. (2015) and Buehner et al. (2015), respectively]. Combined with the arrival, in the GDPS, of incremental analysis updates (i.e., hourly updates to the analyzed fields, over a 6-h window, as opposed to the previously available 6-hourly analyses), the new atmospheric analyses allow smooth and continuously updated wind forcings which are now used to produce a GDWPS pseudoanalysis ensuring higher-quality initial conditions and a smooth transition into the next wave forecast cycle.

b. Global ice–ocean forecasts

In June 2014, GIOPS (Smith et al. 2016) was added to the suite of operational systems run at the Canadian Meteorological Center. It is the result of a coupling between $1/4^\circ$ ocean and ice models. The eddy-permitting ocean model is based on version 3.1 of the Nucleus for European Modeling of the Ocean (NEMO; Madec 2008). The ice component is version 4.0 of the thermodynamic sea ice model Community Ice Code (CICE; Hunke and Lipscomb 2010). The model is run once daily at 0000 UTC to produce 10-day (240 h) forecasts of ocean and ice conditions. The 3-hourly ice concentrations that result from this system are taken to provide the GDWPS with the time varying ice conditions.

5. Validation of the wave forecasts

In this section, wave observations from moored buoys and satellite altimeter data are used to validate and compare the GDWPS to the regional wave forecast systems. We demonstrate the ability of the model to accurately predict significant wave height H_s and peak period T_p in the ocean basins that border Canada. We note that the wave forecasts are evaluated over two periods, from 15 August to 31 October 2014 and from 15 December 2014 to 28 February 2015. In addition, a reforecast of fall of 2012 was performed (after completion of a reforecast of the atmospheric conditions to ensure consistent atmospheric forecasts over all periods and cases for which the GDWPS was evaluated). We note that a more detailed validation of the system, which is required for an operational implementation, is available in CMC (2015).

a. Site-specific forecast

1) PACIFIC

It has long been demonstrated that swell can travel and carry energy across ocean basins such as the Pacific and Atlantic Oceans (e.g., Sverdrup and Munk 1947; Barber and Ursell 1948; Munk et al. 1963; Snodgrass et al. 1966). The regional forecast systems, in addition to relying on a first-order propagation scheme (which is numerically dispersive), were too localized to cover all swell generation areas and periodically resulted in poor forecasts along the North American West Coast. Figure 3 is an example of such events where the regional wave forecast system (blue) is missing the swell information thus leading to poor H_s and T_p forecasts (time series displayed in Fig. 3 show forecast hours 1–36 of predictions issued in intervals of 36 h starting at

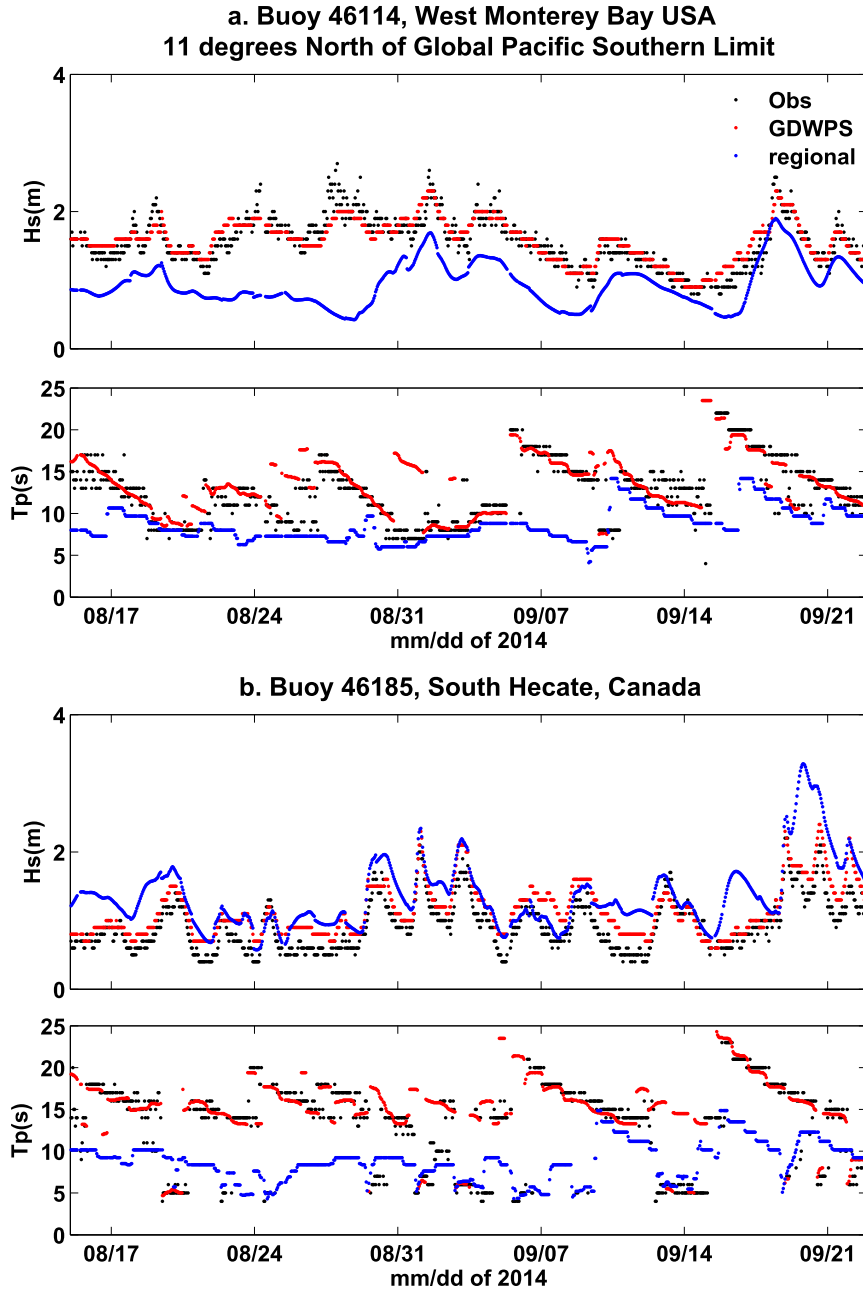


FIG. 3. Time series of observed (black) and forecast significant wave height (m) and peak period (s) for (a) Pacific buoy 46114, West Monterey Bay, United States, and (b) Pacific buoy 46185, South Hecate, Canada. The colored lines show the regional forecast system (blue) and the GDWPS (red) for forecast hours 1–36 from runs issued at intervals of 36 h starting at 0000 UTC 15 Aug 2014.

0000 UTC 15 August 2014). Note how the predicted T_p miss the swell events clearly evident in the observations (black) for which the long waves, the forerunners, arrive followed by gradually shorter waves. In comparison, the GDWPS (Fig. 3, red) offers a much better prediction of both H_s and T_p although it is noted that there are errors in the timing of the arrival

of the swells, similar to those reported by Chawla et al. (2013).

Comparisons of the GDWPS 5-day energy forecasts to observations were also used to allow a qualitative comparison of the forecast and observed wave fields without focusing on the timing of the arrival. Figure 4 shows two representative examples plotted in

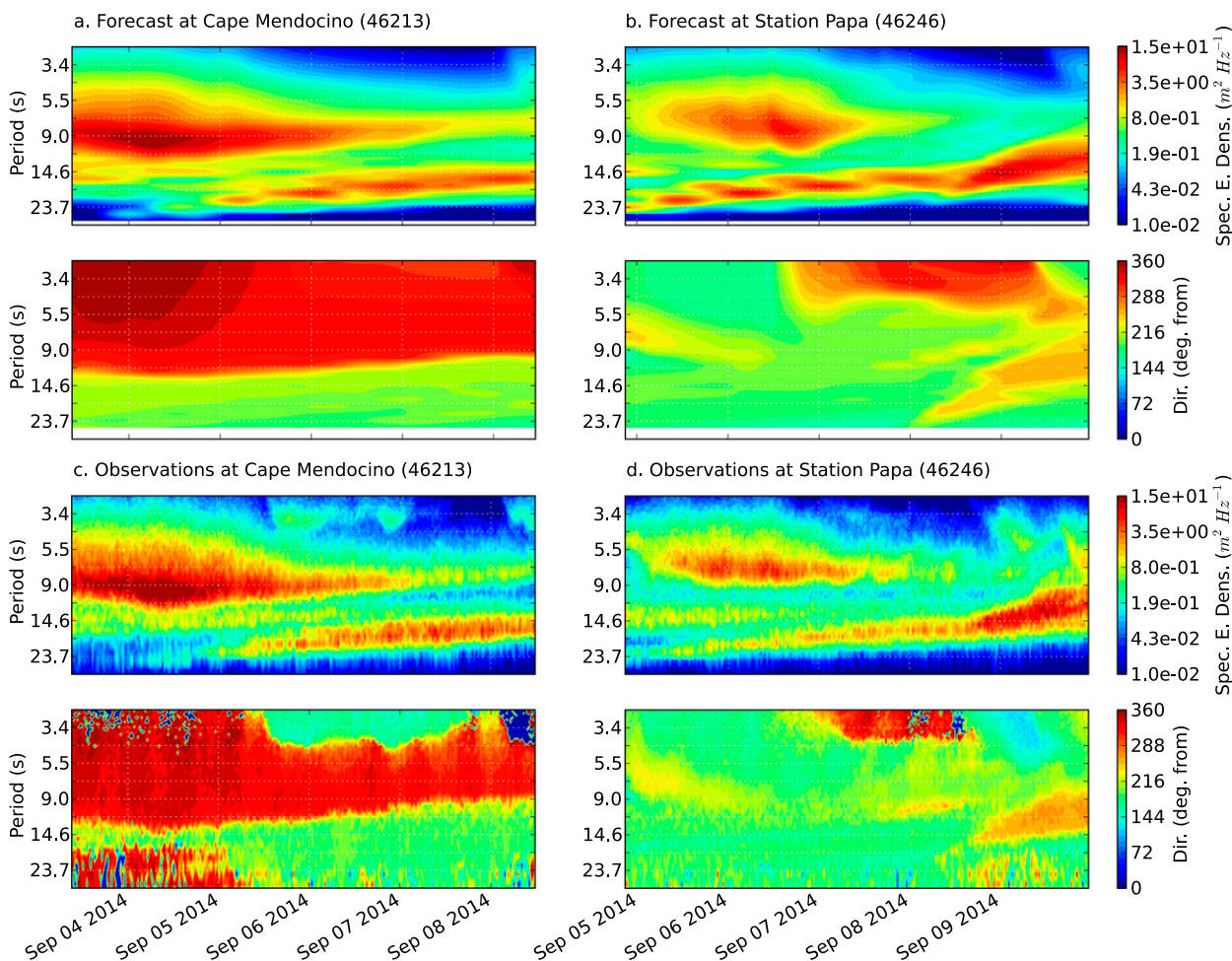


FIG. 4. Spectrograms of wave fields at (left) buoy 46213, Cape Mendocino, United States, and (right) buoy 46246, Ocean Station Papa. (a) The forecast spectral energy density over the 5-day GDWPS issued 1200 UTC 3 Sep 2014 at Cape Mendocino above the GDWPS forecast wave direction. (c) The corresponding observations. (b),(d) As in (a) and (c) for the location Ocean Station Papa and the 5-day GDWPS forecast issued 0000 UTC 5 Sep 2014.

the form of spectrograms where the y axis is the period, the x axis is time, and the colors indicate the spectral energy density (top) or direction (bottom) in each frequency bin (labeled as periods). Note that the range of the y axis has been cropped to focus on the active portion of the spectra. The first example (Fig. 4a) is from buoy 46213, Cape Mendocino in California. The forecast is from 1200 UTC 3 September 2014 and represents one full 5-day forecast. The corresponding observations are shown in Fig. 4c. The second 5-day forecast and corresponding observation (Figs. 4b and 4d, respectively) are from buoy 46246, Ocean Station Papa. The GDWPS forecast was initialized 0000 UTC 5 September 2014. In general, the GDWPS reproduces the observed wave energy for the whole forecast period matching well both the wind and swell seas. Similarly, the wave directions are overall well predicted although some shorter-lived

events are missed such as some of the swell seas at the beginning of the forecast period.

2) ARCTIC

Time series of observed and forecast H_s and T_p are shown in Fig. 5 for two Arctic locations. It is the first time that an operational wave forecast system, at EC, is compared to observations in this basin. The black lines are the observations, other colors mark the forecast lead times where day 1 (red) implies a time series built by concatenating 0–24-h forecasts for the period of interest. In general, the forecasts at all lead times represent well the observed conditions with forecast skill decreasing with increasing forecast lead time. At lead times of 5 days (Fig. 5, green line), changes from one forecast to the next can be large (note the vertical jumps in the forecast line at some 24-h intervals). Peaks continue to

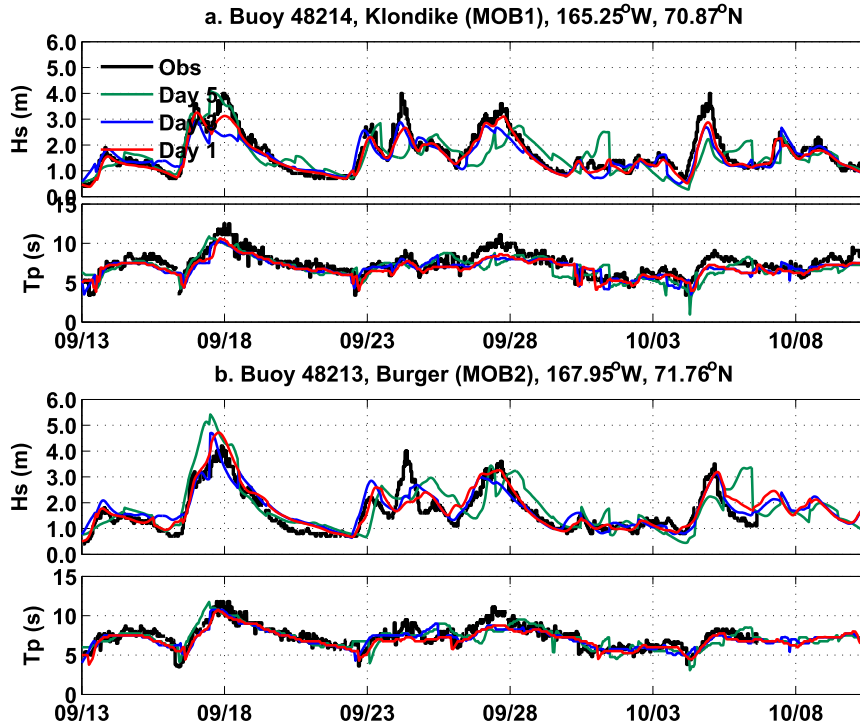


FIG. 5. Time series of observed (black) and forecast significant wave height (m) and peak period (s) for (a) Arctic buoy 48214, Klondike (MOB1), and (b) Arctic buoy 48213, Burger (MOB2). The colored lines indicate the forecast range used to build the forecast time series. Day 1 (red) is a time series created using successive 0000 UTC run forecast hours 1–24. Day 3 (blue) is built using forecast hours 49–72 and day 5 (green) is built using forecast hours 97–120.

be forecast but their amplitude and timing can be off, suggesting that an ensemble forecast system could be used to improve forecast skill.

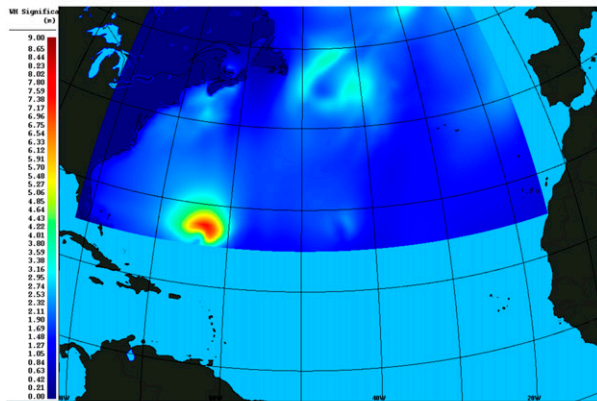
3) ATLANTIC

In the Atlantic basin, tropical storms and hurricanes can reach Canadian waters. In this basin, differences observed between the regional and global forecast systems are due to resolution, as shown in Fig. 6. In the long-range regional forecast system, the grid spacing is coarse. Storms are smoothed by the aggregation of the forcing fields onto the wave grid and resulting Hs fields tend to be underpredicted (Fig. 6a). A lengthy discussion of this effect can be found in Cavaleri (2009). In the short-range regional system (Fig. 6b; higher grid spacing but coarse spectral resolution; see Table 1 for details), the spatial resolution is too high for the spectral resolution and results in a pronounced garden sprinkler effect (GSE; Fig. 6b; the separation of the wave field into several discrete wave fields with distance from the source). For some of the short-range regional wave forecasts produced during hurricane conditions, the amplitude of the GSE was found to exceed 1 m. In the GDWPS, the spectral resolution has been increased and

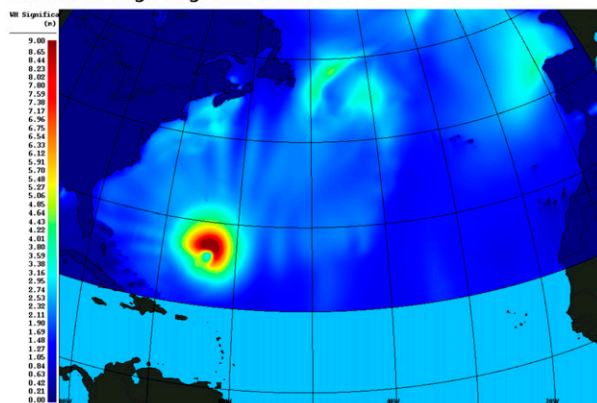
combined with the GSE alleviation of Tolman (2003); the problem is now well under control as is shown in Fig. 6c (note that the shadow in the forecast wave field is not due to the GSE but rather to the presence of Bermuda).

Figure 7 is another example of a well forecast hurricane. Figure 7a shows one of the GDWPS forecasts during the 2012 Hurricane Sandy. Figures 7c–f also show the observed (black) and forecast GDWPS Hs for the four buoys marked with yellow dots in Fig. 7a. Here the colors identify the forecast lead time at the time of maximum Hs. Thus, a day 1 forecast implies that the maximum Hs occurs within the first 24 h of the forecast period. A closer look at the maximum forecast Hs is shown in Fig. 7b for all buoys influenced by Sandy that recorded maximum Hs in excess of 4 m. For these locations, a Q–Q plot of the maximum observed and forecast Hs (after allowing for timing errors of up to 3 h) are shown for three lead times. The black line is the unit-slope line. At short lead times (e.g., maximum Hs observed within the first 24 h of the forecast; Fig. 7b red line), there is a tendency to slightly underestimate the peaks. This tendency is reversed with increasing lead times when the tendency is to overforecast maximum

a. Long-range regional forecast



b. Short-range regional forecast



c. GDWPS

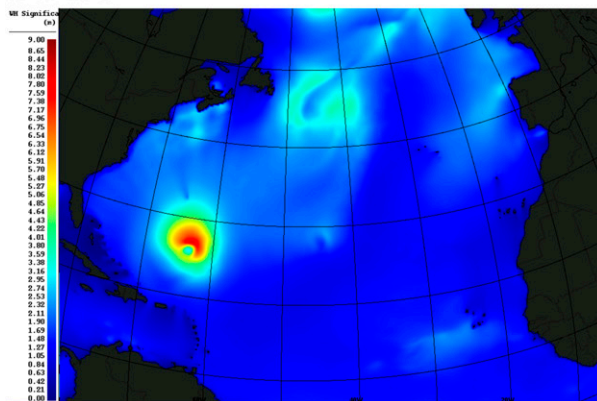


FIG. 6. Forecast of Hurricane Leslie wave fields (24-h forecast issued at 0000 UTC 5 Sep 2012, valid 0000 UTC 6 Sep 2012) produced with the (a) long-range (coarse grid spacing, coarse spectral resolution) regional forecast system, (b) the short-range (smaller grid spacing, coarse spectral resolution), and (c) GDWPS (intermediate grid spacing, intermediate spectral resolution). See Table 1 for a detailed list of grid spacings and spectral discretizations.

Hs. Uncertainties in the amplitude and timing of the peak Hs increase with increasing lead time, in general agree with the observed increase in the variance of atmospheric forecast errors. It is also noted that even

though the intensity of a storm may be accurately predicted long before it occurs, small errors in its location and trajectory can influence the timing and amplitude of the forecast waves. This suggests that the deterministic system should be complemented with an ensemble system to move from a discrete time and amplitude event forecast to a window of probable time and amplitude forecast. The added value of ensemble wave systems was recently demonstrated for the case of Hurricane Sandy by Magnusson et al. (2014) and Alves et al. (2015). A global ensemble system is under development at Environment Canada.

b. Seasonal statistics

1) VALIDATION AGAINST MOORED BUOY OBSERVATIONS

The regional wave forecast systems and the GDWPS were also compared over seasons. For the Pacific and Atlantic regions (there are no in situ records available within the regional domain of the Arctic basin), the statistics were computed for every forecast hour, using all buoys common to both the regional systems and the GDWPS. Figure 8 shows the bias (first column), the standard deviation of forecast error (STDE, second column), the scatter index [SI (root-mean-square error normalized with mean observed wave height), third column], and correlation coefficient (last column) for the long-range Pacific domain. The fall period (from 15 August to 31 October 2014) is shown in the top half. The winter season (from 15 December 2014 to 28 February 2015) is shown in the bottom half. The long-range regional systems scores are shown in blue whereas the GDWPS scores are in red. For Hs, the GDWPS brings remarkable improvements over the regional system. For example, during the fall season, the STDE and SI of the regional 0-h forecast are comparable to the 48-h GDWPS scores. In winter, when swell seas no longer dominate, the gain in Hs skill is reduced to roughly 12 h (although it must be noted that the refinement of the wave field is much improved, similar to what was shown in Fig. 6 between the long-range Atlantic and the GDWPS forecast). The scores for the peak period T_p suggest a degradation in the quality of the GDWPS forecast over the regional forecast. This is actually not the case. It is an artifact of the double penalty for forecasting the arrival of swell events before they are actually observed (errors are large for forecasting the fields too early and large again for not forecasting them at the time when they actually occur). This is illustrated in Figs. 9a and 9b using a $Q-Q$ plot for the two Pacific time series discussed in Fig. 3 and in Fig. 9c for all buoys located in the northeast Pacific. At stations directly

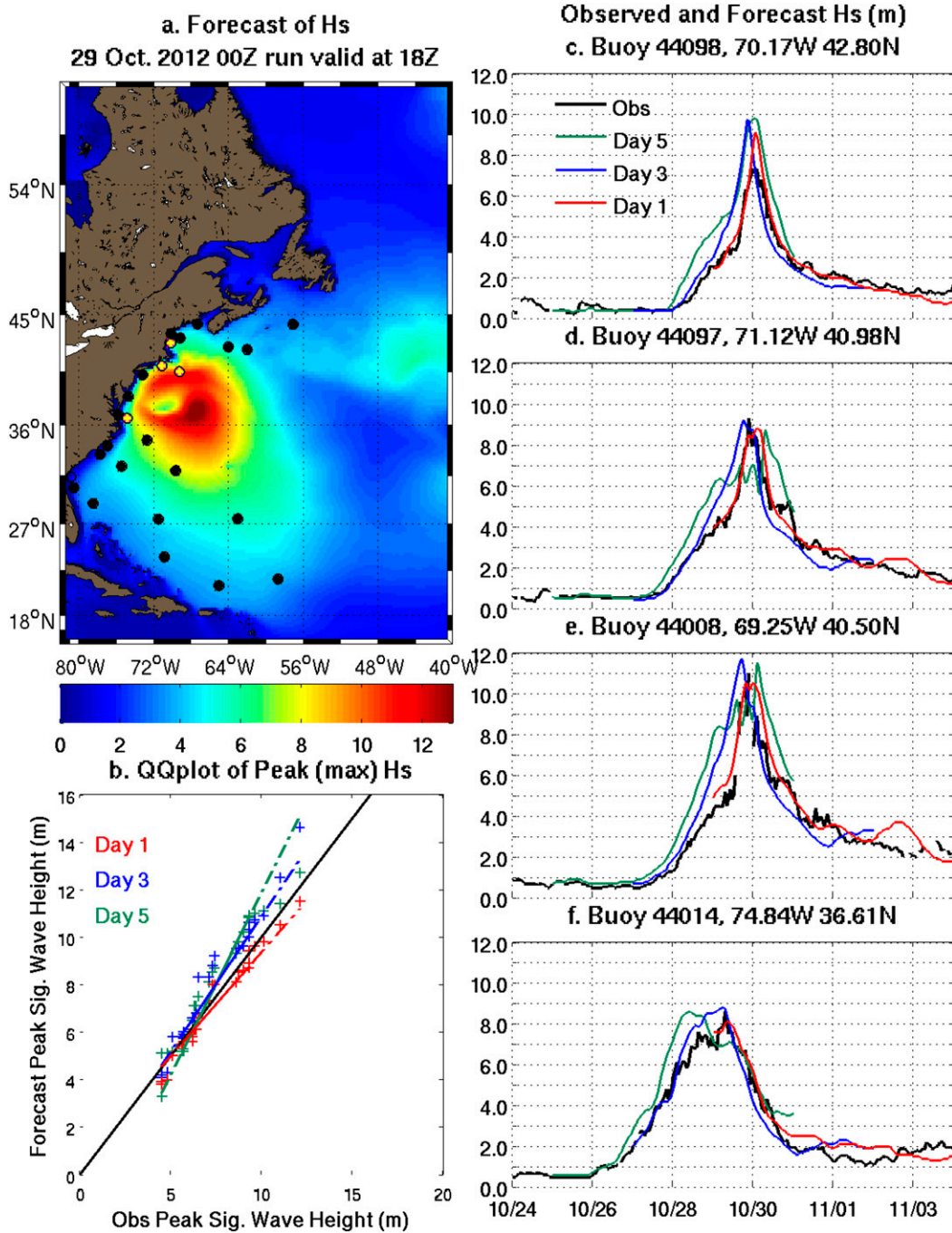


FIG. 7. Wave forecast during Hurricane Sandy (26–31 Oct 2012). (a) The forecast wave field at 1800 UTC 29 Oct 2012. The dots mark buoys which recorded Hs > 4 m between 0000 UTC 26 Oct and 2300 UTC 31 Oct. (b) *Q*–*Q* plot of observed and corresponding forecast maximum Hs (within ±3 h of observed peak) over the period 26–31 Oct, computed for several lead times: red is for peaks observed within the first 24 h of forecast, blue is for lead times within hours 49–72, and green for lead times between 97 and 120 h. (c)–(f) The observed and forecast Hs at four buoys marked by yellow dots in (a). Lead times (colored lines) mark the forecast range at the time of observed peak Hs.

exposed to incoming swell seas (e.g., Figs. 9a and 9b), the regional systems clearly fail to reproduce the full range of observed values (note that the *Q*–*Q* plot displays the range of forecast and observed values irrelevant of their

time of occurrence thereby removing the effect of timing errors). Combining all buoys east of station Papa (including those sheltered from direct exposure to the swell seas) lessens the issue but the overall tendency of the

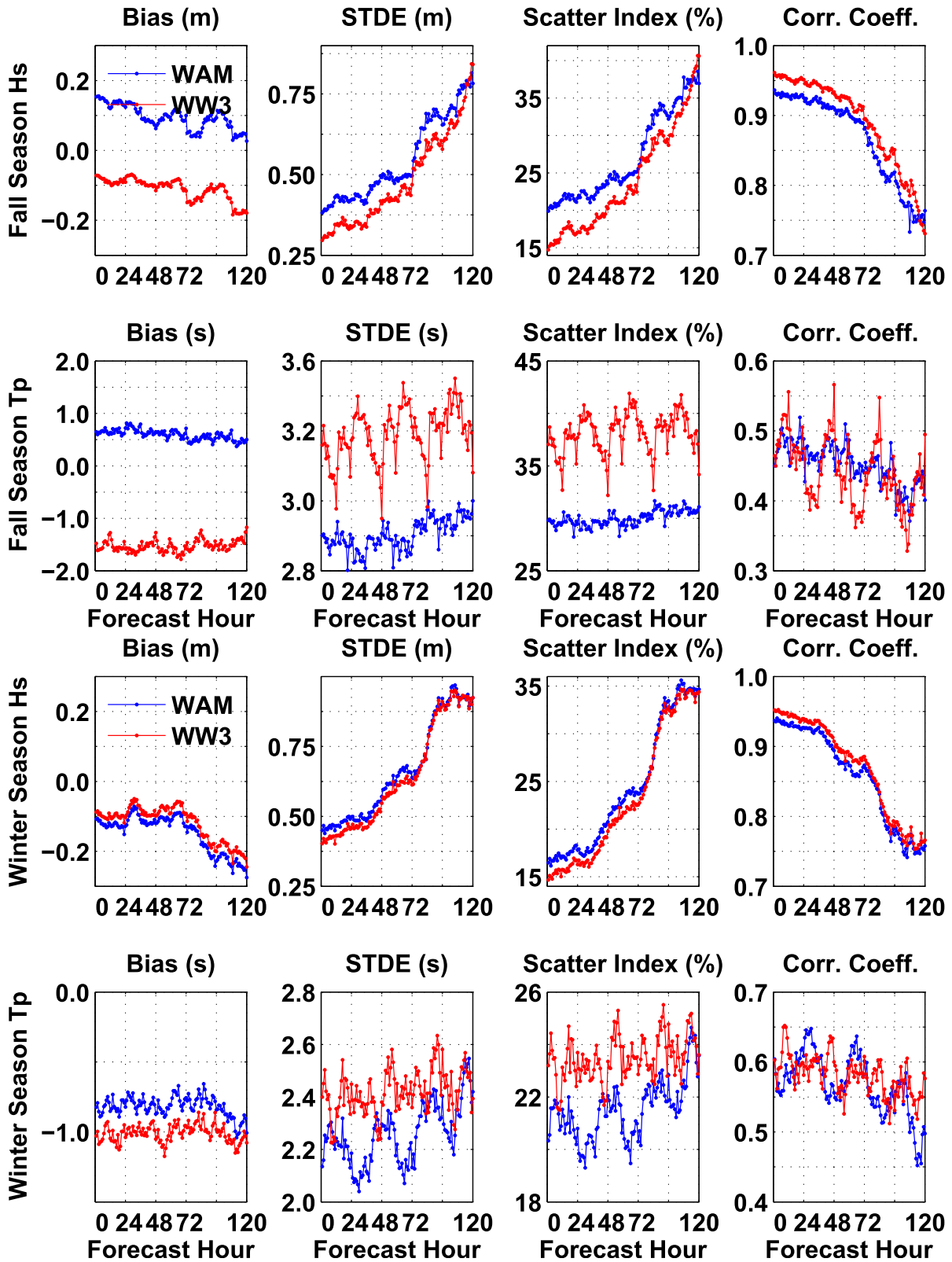
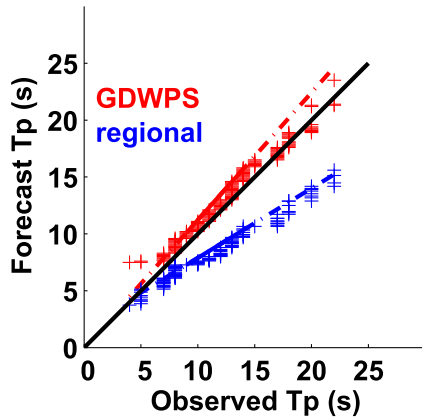
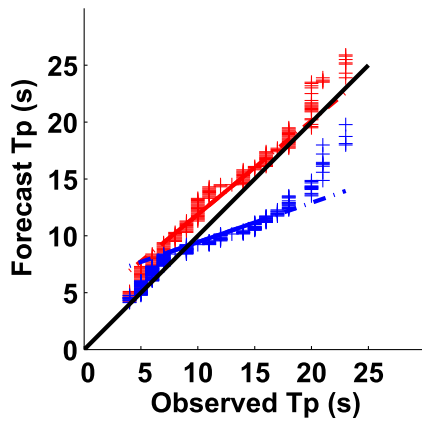


FIG. 8. Pacific regional domain statistics calculated using buoy data and regional long-range Pacific (labeled WAM, blue) and GDWPS (labeled WW3, red) for (first row) Hs and (second row) Tp for the fall season (from 15 Aug to 31 Oct 2014). (third row) Hs and (fourth row) Tp are the same for the winter season (from 15 Dec 2014 to 28 Feb 2015). (left)–(right) The bias, the standard deviation of the error, the scatter index, and the correlation coefficient.

a. Buoy 46114, West Monterey Bay USA



b. Buoy 46185, South Hecate, Canada



c. North East Pacific Buoys

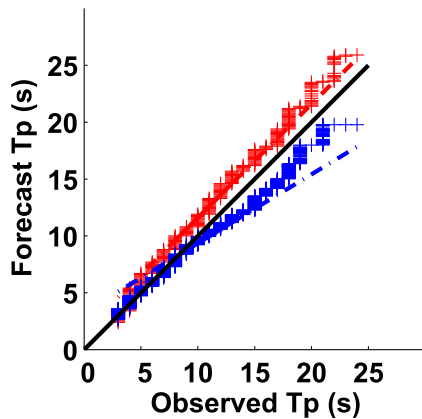


FIG. 9. A $Q-Q$ plot of the observed peak period (x axis) and GDWPS (y axis; red) and regional (y axis; blue) forecast peak period. All 120 h of forecast and corresponding observations for the fall 2014 period are shown for (a) Pacific buoy 46114, West Monterey Bay, United States; (b) Pacific buoy 46185, South Hecate, Canada; and (c) all northeast Pacific buoys (including Ocean Station Papa and all other eastern buoys).

regional system to underestimate the large swell remains (Fig. 9c). For several of these stations, the regional system that misses swell information generated outside of its small domain, predicting shorter but consistent values of T_p , is found to have overall smaller errors. Figure 10 shows the same set of scores as Fig. 8 but for the short-range Atlantic system (blue) and the GDWPS (red). It is noted that there are no comparable swells affecting the Atlantic buoys used for validation and so the double penalty discussed above no longer dominates the error signal. The short-range Atlantic system is considered by forecasters to be the better of the two Atlantic regional domains in place. Overall, the improvement in forecast skill is roughly 24 h with the GDWPS STDE and SI showing a reduction of approximately 15% over the full short-range forecast period.

2) VALIDATION AGAINST SATELLITE ALTIMETER DATA

A broader validation was also performed using satellite altimeter data for the fall season (note that the merged dataset was not yet available for the winter period at the time these statistics were computed). The observation and forecasts are matched by interpolating (spatially) the forecasts to the observation location. There is no temporal interpolation. For a given time of observation, the forecast from the nearest forecast hour is used (hence the forecast matching the time of observation ± 30 min). Several error statistics are then computed for each pair of observation and forecast and for various lead times. The data are then aggregated in bins of $2^\circ \times 2^\circ$ over windows of 24 h (e.g., all pairs of matching observation and forecast for which the lead time is between 1 and 24 h). Statistics over a bin are computed only if more than 60 pairs are available within that bin (increasing the minimum number of pairs to 100 removes most of the Canadian Arctic bins). An example of results for the scatter index over the first 24 h window is shown in Fig. 11. Figure 11a shows the scatter index for the forecasts produced using the long-range regional Pacific forecast system. In Figs. 11b and 11c, the short-range Arctic and Atlantic systems are shown respectively. Because the short-range systems are driven with higher-resolution winds and updated more frequently (four times daily), it is generally assumed that they result in more accurate forecasts. In fact, comparing the long-range and short-range Arctic or Atlantic grids yields a checkerboard pattern. The number of bins with smaller scatter index in the short-range regional systems only barely exceeds the number of bins with smaller scatter index in the long-range system (at most, 10 bins overall separate the systems; not shown). Figures 11d–f show the scatter index for

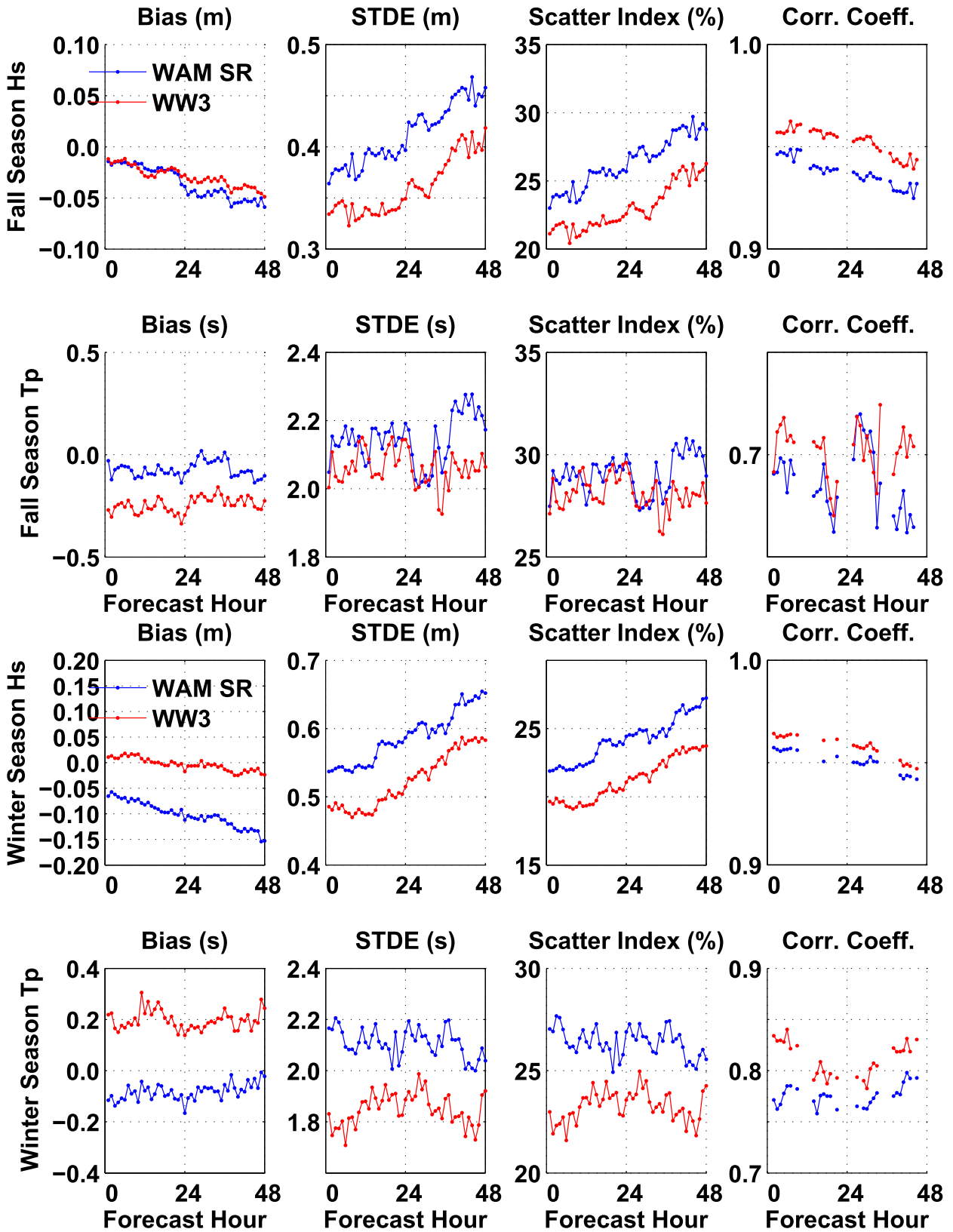


FIG. 10. As in Fig. 8 but for Atlantic regional domain statistics. The regional short range (labeled WAM, blue) is used.

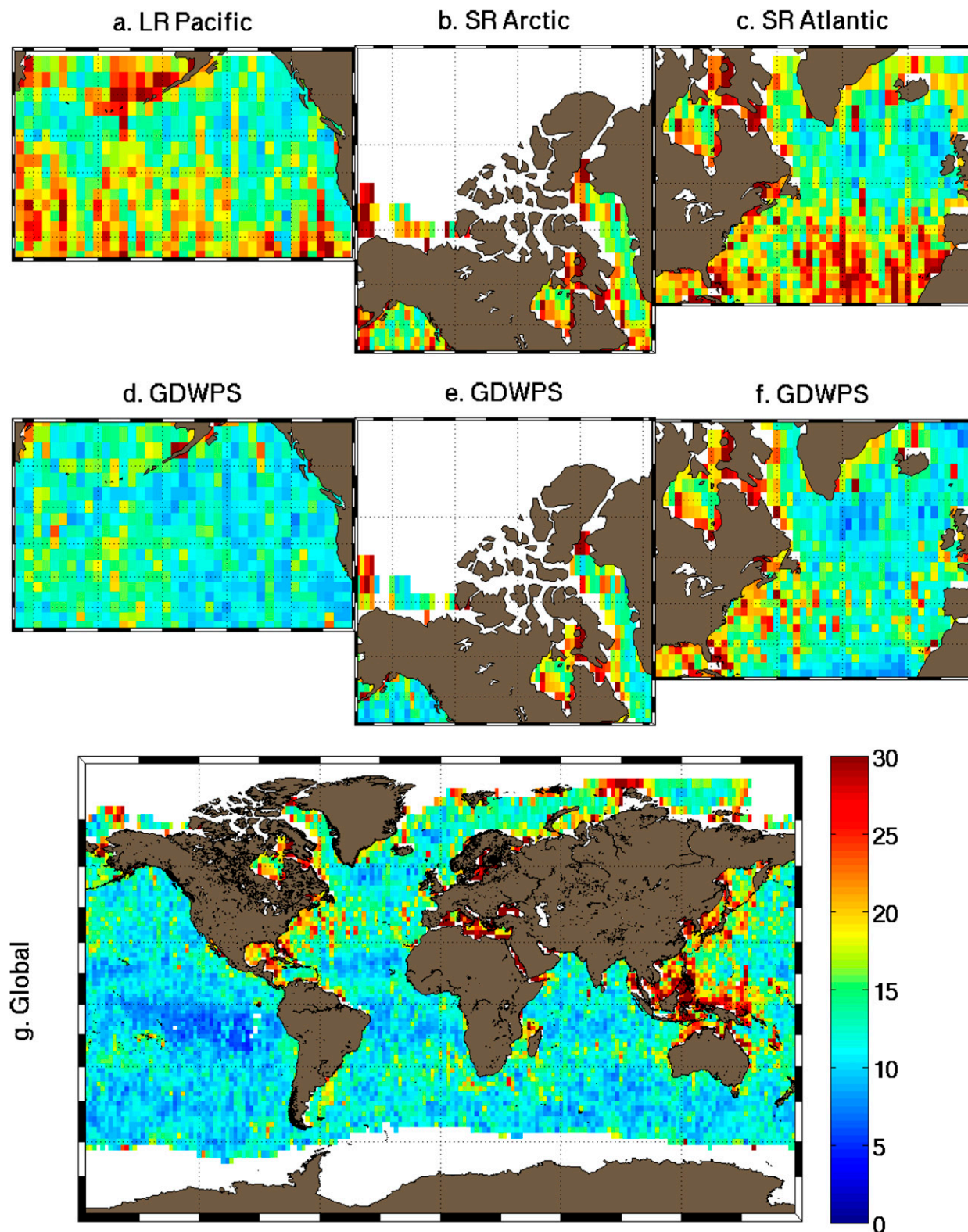


FIG. 11. Scatter index (%) calculated using forecast waves interpolated to the satellite observation position. The period shown is fall (15 Aug–31 Oct 2014). Results are averaged over forecast times from 1 to 24 h in $2^\circ \times 2^\circ$ bins. Domains shown are (a) long-range Pacific, (b) short-range Arctic, (c) short-range Atlantic, (d)–(f) GDWPS over the same areas as in (a)–(c), and (g) full domain of the GDWPS. The colorbar applies to all panels.

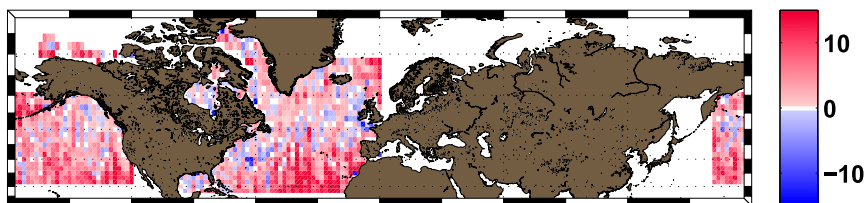


FIG. 12. Scatter index difference (%) over common regional and GDWPS forecast regions. Where statistics from both the Arctic and Pacific grids exist, the Pacific grid is kept. The same applies to the Atlantic domain. The GDWPS scatter index is then subtracted from the regional scatter indexes. Colors indicate the difference. Red tones (78% of the bins) indicate bins where the regional grids have a larger scatter index than the GDWPS. Blue tones are the opposite.

the GDWPS zoomed over the regional domains. The full global domain is shown in Fig. 11g. The color scales are the same for all panels. In general, the GDWPS SI is smaller over all regional domains, confirming that regional forecast skill is improved with the GDWPS. The GDWPS is also shown to perform well in other parts of the world's oceans.

The scatter index statistics of the regional systems were also compared to those of the GDWPS by taking their difference at each common bin (since some regional domains overlap, the Arctic grid results are used only outside of the Pacific and Atlantic regional domains). The GDWPS was found to have a smaller scatter index in 78% of bins for which a regional forecast exists. Results are summarized in Fig. 12 where red tones indicate that the GDWPS forecast has a smaller scatter index than the regional system. Other statistics such as the normalized root-mean-square error (not shown) show the same overall pattern.

6. Summary and discussion

A global deterministic wave prediction system (GDWPS) has been described. The new GDWPS is the first step taken toward a full redesign of the operational wave forecast systems in place at Environment Canada. Based on validation against buoy observation and satellite altimeter data for the period from 15 August to 31 October 2014 and from 15 December 2014 to 28 February 2015, the GDWPS has been shown to improve on the regional forecast previously used in operations. It also has the distinct advantage of replacing five regional systems with a single system, thus reducing the cost of maintenance.

It is important to note that although the regional systems described in this article are based on WAM whereas the GDWPS is based on WW3, this should not be considered as a comparison of these wave models. The overall design of the regional (WAM based) systems was limited in many aspects (e.g., inadequate

spatial coverage, coarse spectral resolution, poor handling of the forcing fields, etc.). Their seemingly poorer forecast skills are thus not surprising and should not be attributed to the model itself.

Examples of time series of significant wave height H_s and peak period T_p at select buoys (Fig. 3) and spectrograms (Fig. 4) demonstrate that the long known problem of poorly forecast swells in the northeast Pacific has been addressed. It is in this region that the GDWPS was shown to bring the most significant improvements. In the fall season, the forecast skill was shown to have improved by as much as 48 h (Fig. 8). This implies that a forecast issued today with the GDWPS, valid in 48 h, is as skillful as the forecast that will be issued by the regional system in 48 h, for immediate validity.

The first-ever validation of Canadian operational wave forecasts within the Arctic was shown in Fig. 5. Time series of H_s and T_p at two buoys were used to demonstrate that the GDWPS also has skill in the Arctic. Satellite validation complemented this buoy-based validation (Fig. 11). Although the scores tend to be noisier near the ice edge, in part owing to the sparsity of pairs of observation and forecast within each bin, the GDWPS appears to perform adequately in the Arctic Ocean and to provide improved numerical wave guidance over the regional short-range and long-range systems previously in place (Fig. 12). It is noted that the addition of time-evolving ice fields is difficult to evaluate. GIOPS ice cover forecasts have been shown by Smith et al. (2016) to improve over the persistence of the initial condition (the equivalent of using a static analysis). Areas of open water and the location of the marginal ice zone (the zone between open and ice-covered water) are in general better forecast throughout the first several days of integration. The impact on the wave forecast is not easily measurable at this time; it follows, however, that any improvement in the representation of the ice cover implies that areas where waves can occur are better represented.

The GDWPS was also shown to produce realistic wave forecasts under tropical cyclone conditions. The systematic underforecasting of the wave fields in the long-range Atlantic system and the garden sprinkler effect evident in the short-range Atlantic system were shown to be corrected with the GDWPS (Fig. 6). The GDWPS was further evaluated for Hurricane Sandy (Fig. 7) and shown to produce realistic forecasts of extreme wave conditions.

It was noted in the evaluation of the GDWPS at longer lead times (Fig. 3 and Fig. 7) that forecast errors, in the timing and amplitude of waves, increased rapidly with increasing lead time. Part of this error growth is due to larger uncertainty in the forcing fields. With increasing lead times, the trajectory, intensity, and size of storms are less accurate. Small changes in the initial conditions of the atmospheric systems can have a considerable impact on a storm several days into the forecast period. A global wave ensemble forecast system is thus under development to improve wave forecast skill at long forecast ranges by replacing deterministic forecasts with probabilistic forecasts. Such an approach has been shown to be successful for other wave forecast (e.g., Alves et al. 2013) and sea level forecast (e.g., Bernier and Thompson 2015) systems.

The development of the wave ensemble forecast system will soon be followed by the addition of properly nested regional domains bringing higher-resolution forecasts around the Canadian coastlines. Completely revamped systems are also under evaluation for the Great Lakes region. Finally, coupled wave–atmosphere and wave–ice forecast systems are under development.

Acknowledgments. The authors thank reviewers whose comments were very valuable. NBB also thanks PERD B11.001 and SARNif SN201222 for financial support.

REFERENCES

- Alves, J.-H., and Coauthors, 2013: The NCEP–FNMOCC combined wave ensemble product: Expanding benefits of interagency probabilistic forecasts to the oceanic environment. *Bull. Amer. Meteor. Soc.*, **94**, 1893–1905, doi:10.1175/BAMS-D-12-00032.1.
- , S. Stripling, A. Chawla, H. Tolman, and A. van der Westhuysen, 2015: Operational wave guidance at the U.S. National Weather Service during tropical/post-Tropical Storm Sandy, October 2012. *Mon. Wea. Rev.*, **143**, 1687–1702, doi:10.1175/MWR-D-14-00143.1.
- Amante, C., and B. W. Eakins, 2009: ETOPO1 1 Arc-Minute Global Relief Model: Procedures, data sources and analysis. NOAA Tech. Memo. NESDIS NGDC-24, 19 pp. [Available online at <https://www.ngdc.noaa.gov/mgg/global/relief/ETOPO1/docs/ETOPO1.pdf>.]
- Ardhuin, F., and Coauthors, 2010: Semiempirical dissipation source functions for ocean waves. Part 1: Definition, calibration, and validation. *J. Phys. Oceanogr.*, **40**, 1917–1941, doi:10.1175/2010JPO4324.1.
- Barber, N. F., and F. Ursell, 1948: The generation and propagation of ocean waves and swell. I. Wave periods and velocities. *Philos. Trans. Roy. Soc. London*, **240A**, 527–560, doi:10.1098/rsta.1948.0005.
- Battjes, J. A., and J. P. F. M. Janssen, 1978: Energy loss and set-up due to breaking of random waves. *Proc. 16th Conf. on Coastal Engineering*, Hamburg, Germany, ASCE, 569–587. [Available online at <http://repository.tudelft.nl/assets/uuid:2fba43fe-f8bd-42ac-85ee-848312d2e27e/BattjesJanssen.pdf>.]
- Bernier, N. B., and K. R. Thompson, 2015: Deterministic and ensemble storm surge prediction for Atlantic Canada with lead times of hours to ten days. *Ocean Modell.*, **86**, 114–127, doi:10.1016/j.ocemod.2014.12.002.
- Bidlot, J.-R., 2012: Present status of wave forecasting at E.C.M.W.F. *Proc. ECMWF Workshop on Ocean Waves*, Reading, United Kingdom, ECMWF, 16 pp. [Available online at http://old.ecmwf.int/publications/library/ecpublications/_pdf/workshop/2012/Ocean_Waves/Bidlot.pdf.]
- , D. Holmes, P. Wittmann, R. Lalbeharry, and H. Chen, 2002: Intercomparison of the performance of operational ocean wave forecasting systems with buoy data. *Wea. Forecasting*, **17**, 287–310, doi:10.1175/1520-0434(2002)017<0287:IOTPOO>2.0.CO;2.
- , and Coauthors, 2007: Intercomparison of operational wave forecasting systems. *Proc. 10th Int. Workshop on Wave Hindcasting and Forecasting*, Oahu, HI, JCOMM, H1. [Available online at http://www.waveworkshop.org/10thWaves/Papers/paper_10th_workshop_Bidlot_at_al.pdf.]
- Buehner, M., and Coauthors, 2015: Implementation of deterministic weather forecasting systems based on ensemble-variational data assimilation at Environment Canada. Part I: The global system. *Mon. Wea. Rev.*, **143**, 2532–2559, doi:10.1175/MWR-D-14-00354.1.
- Caron, J.-F., T. Milewski, M. Buehner, L. Fillion, M. Reszka, S. Macpherson, and J. St-James, 2015: Implementation of deterministic weather forecasting systems based on ensemble-variational data assimilation at Environment Canada. Part II: The regional system. *Mon. Wea. Rev.*, **143**, 2560–2580, doi:10.1175/MWR-D-14-00353.1.
- Cavaleri, L., 2009: Wave modeling—Missing the peaks. *J. Phys. Oceanogr.*, **39**, 2757–2778, doi:10.1175/2009JPO4067.1.
- CBCNews, 2012: Ocean Ranger sinking still haunts 30 years later. [Available online at <http://www.cbc.ca/news/canada/newfoundland-labrador/ocean-ranger-sinking-still-haunts-30-years-later-1.1181316>.]
- , 2013: Woods Harbour, N.S., plans funerals for missing fishermen. [Available online at <http://www.cbc.ca/news/canada/nova-scotia/woods-harbour-n-s-plans-funerals-for-missing-fishermen-1.1321502>.]
- Charney, J. G., and N. A. Phillips, 1953: Numerical integration of the quasi-geostrophic equations for barotropic and simple baroclinic flows. *J. Meteor.*, **10**, 71–99, doi:10.1175/1520-0469(1953)010<0071:NIOTQG>2.0.CO;2.
- Chawla, A., and H. L. Tolman, 2007: Automated grid generation for WAVEWATCH III. NCEP/NOAA/NWSm Tech. Note 254, 71 pp. [Available online at http://polar.ncep.noaa.gov/mmab/papers/tn254/MMAB_254.pdf.]
- , and H. Tolman, 2008: Obstruction grids for spectral wave models. *Ocean Modell.*, **22** (1–2), 12–25, doi:10.1016/j.ocemod.2008.01.003.
- , and Coauthors, 2013: A multigrid wave forecasting model: A new paradigm in operational wave forecasting. *Wea. Forecasting*, **28**, 1057–1078, doi:10.1175/WAF-D-12-00007.1.

- CMC, 2012: Improvements to the Regional Deterministic Wave Prediction System (RDWPS 2.0) with the wave model WAM-EC version 4.5.1. Canadian Meteorological Centre of Environment Canada Tech. Rep., 94 pp. [Available online at http://collaboration.cmc.ec.gc.ca/cmc/cmci/product_guide/docs/lib/op_systems/doc_opchanges/technote_rdwps_20120524_e.pdf.]
- , 2015: Experimental implementation of the Global Deterministic Wave Prediction System (GDWPS) version 1.0.0. Canadian Meteorological Centre of Environment Canada Tech. Rep., 50 pp.
- Côté, J., J. Desmarais, S. Gravel, A. Méthot, A. Patoine, M. Roch, and A. Staniforth, 1998a: The operational CMC–MRB Global Environmental Multiscale (GEM) model. Part II: Results. *Mon. Wea. Rev.*, **126**, 1397–1418, doi:10.1175/1520-0493(1998)126<1397:TOCMGE>2.0.CO;2.
- , S. Gravel, A. Méthot, A. Patoine, M. Roch, and A. Staniforth, 1998b: The operational CMC–MRB Global Environmental Multiscale (GEM) model. Part I: Design considerations and formulation. *Mon. Wea. Rev.*, **126**, 1373–1395, doi:10.1175/1520-0493(1998)126<1373:TOCMGE>2.0.CO;2.
- Girard, C., and Coauthors, 2014: Staggered vertical discretization of the Canadian Environmental Multiscale (GEM) model using a coordinate of the log-hydrostatic-pressure type. *Mon. Wea. Rev.*, **142**, 1183–1196, doi:10.1175/MWR-D-13-00255.1.
- Hasselmann, K., and Coauthors, 1973: Measurements of wind-wave growth and swell decay during the Joint North Sea Wave Project (JONSWAP). *Deutschen Hydrographischen Zeitschrift Reihe A (80)*, Nr. 12, 95 pp. [Available online at <http://repository.tudelft.nl/assets/uuid:f204e188-13b9-49d8-a6dc-4fb7c20562fc/Jonswap-Hasselmann1973.pdf>.]
- Hasselmann, S., K. Hasselmann, J. Allender, and T. Barnett, 1985: Computations and parameterizations of the nonlinear energy transfer in a gravity-wave spectrum. Part II: Parameterizations of the nonlinear energy transfer for application in wave models. *J. Phys. Oceanogr.*, **15**, 1378–1391, doi:10.1175/1520-0485(1985)015<1378:CAPOTN>2.0.CO;2.
- Hunke, E. C., and W. H. Lipscomb, 2010: CICE: The Los Alamos Sea Ice Model documentation and software user's manual version 4.1. Los Alamos National Laboratory Tech. Rep. LA-CC-06-012, 76 pp. [Available online at http://csdms.colorado.edu/w/images/CICE_documentation_and_software_user's_manual.pdf.]
- Khandekar, M. L., and R. Lalbeharry, 1996: An evaluation of Environment Canada's operational wave model based on moored buoy data. *Wea. Forecasting*, **11**, 137–152, doi:10.1175/1520-0434(1996)011<0137:AEOECO>2.0.CO;2.
- Li, J.-G., and A. Saulter, 2014: Unified global and regional wave model on a multi-resolution grid. *Ocean Dyn.*, **64**, 1657–1670, doi:10.1007/s10236-014-0774-x.
- Madec, G., 2008: NEMO reference manual, ocean dynamics component: NEMO-OPA. Preliminary version. Institut Pierre-Simon Laplace (IPSL) Note du Pole de Modélisation, No. 27, 1288–1619.
- Magnusson, L., J.-R. Bidlot, S. Land, A. Thorpe, N. Wedi, and M. Yamaguchi, 2014: Evaluation of the medium-range forecasts for Hurricane Sandy. *Mon. Wea. Rev.*, **142**, 1962–1981, doi:10.1175/MWR-D-13-00228.1.
- Munk, W. H., G. R. Miller, F. E. Snodgrass, and N. F. Barber, 1963: Directional recording of swell from distant storms. *Philos. Trans. Roy. Soc. London*, **255A**, 505–584, doi:10.1098/rsta.2013.0039.
- Out of Gloucester, 1991: The *Andrea Gail*. [Available online at <http://www.downtosea.com/1976-2000/angail.htm>.]
- Queffelec, P., 2004: Long-term validation of wave height measurements from altimeters. *Mar. Geod.*, **27**, 495–510, doi:10.1080/01490410490883478.
- Rogers, W., J. Dykes, and P. Wittmann, 2014: US Navy global and regional wave modeling. *Oceanography*, **27**, 56–67, doi:10.5670/oceanog.2014.68.
- Smith, G., and Coauthors, 2016: Sea ice forecast verification in the Canadian Global Ice Ocean Prediction System. *Quart. J. Roy. Meteor. Soc.*, doi:10.1002/qj.2555, in press.
- Snodgrass, F. E., G. W. Groves, K. F. Hasselmann, G. R. Miller, W. H. Munk, and W. H. Powers, 1966: Propagation of ocean swell across the Pacific. *Philos. Trans. Roy. Soc. London*, **259A**, 431–497, doi:10.1098/rsta.1966.0022.
- Sverdrup, H. U., and W. H. Munk, 1947: Wind, sea, and swell: Theory of relations for forecasting. U.S. Hydrographic Office Tech. Rep. 601, 44 pp. [Available online at <https://archive.org/details/windseaswelltheo00sver/>.]
- The Daily Colonist, 1904: Fifty-six find watery graves. [Available online at <http://archive.org/stream/dailycolonist19040110uvic/19040110#page/n0/mode/1up>.]
- The WAMDI Group, 1988: The WAM model—A third generation ocean wave prediction model. *J. Phys. Oceanogr.*, **18**, 1775–1810, doi:10.1175/1520-0485(1988)018<1775:TWMTGO>2.0.CO;2.
- Tolman, H. L., 2003: Treatment of unresolved islands and ice in wind wave models. *Ocean Modell.*, **5**, 219–231, doi:10.1016/S1463-5003(02)00040-9.
- , 2008: A mosaic approach to wind wave modeling. *Ocean Modell.*, **25**, 35–47, doi:10.1016/j.ocemod.2008.06.005.
- , M. L. Banner, and J. M. Kaihatu, 2013: The NOPP operational wave model improvement project. *Ocean Modell.*, **70**, 2–10, doi:10.1016/j.ocemod.2012.11.011.
- , and Coauthors, 2014: User manual and system documentation of WAVEWATCH III version 4.18. NOAA/NWS/NCEP/MMAB Tech. Note 316, 311 pp. [Available online at <http://polar.ncep.noaa.gov/waves/wavewatch/manual.v4.18.pdf>.]
- Transportation Safety Board of Canada, 2010: Statistical summary marine occurrences 2010. Transportation Safety Board of Canada Tech. Rep. TU1-1/2010E, 21 pp. [Available online at <http://www.tsb.gc.ca/eng/stats/marine/2010/ss10.pdf>.]
- Wessel, P., and W. Smith, 1996: A global, self-consistent, hierarchical, high-resolution shoreline database. *J. Geophys. Res.*, **101**, 8741–8743, doi:10.1029/96JB00104.